AJNR

Histopathologic Characteristics of a Chronic Arteriovenous Malformation in a Swine Model: Preliminary Study

Tarik F. Massoud, Harry V. Vinters, Kuo H. Chao, Fernando Viñuela and Reza Jahan

AJNR Am J Neuroradiol 2000, 21 (7) 1268-1276
http://www.ajnr.org/content/21/7/1268

AJNR Am J Neuroradiol 21:1268–1276, August 2000

Histopathologic Characteristics of a Chronic Arteriovenous Malformation in a Swine Model: Preliminary Study

Tarik F. Massoud, Harry V. Vinters, Kuo H. Chao, Fernando Viñuela, and Reza Jahan

BACKGROUND AND PURPOSE: **The experimental induction of histologic transformations in microvessels of similar caliber to those of nidus vessels of cerebral arteriovenous malformations (AVMs) has not been attempted previously. Our goal was to examine preliminarily the histopathologic characteristics of nidus vessels and the angiographic features of a chronic AVM model in swine.**

METHODS: **AVM models were fashioned from bilateral carotid retia mirabilia of seven swine after the surgical formation of large unilateral carotid-jugular fistulas. One AVM model was made for immediate use, whereas in the other six, follow-up angiography was obtained at varying intervals (2 to 180 days) after model creation. Light and electron microscopy, immunohistochemistry (using monoclonal antibodies against smooth muscle actin and PC10 against proliferating cell nuclear antigen), and histometry were performed on the nidus vessels of three swine: one acutely created, one 2 months old, and one 6 months old.**

RESULTS: **Vascular dilatation and tortuosity of the main arterial feeder and draining vein were evident angiographically as early as 4 days after AVM creation, and were maximal in the 6-month-old model. Compared with the acutely created nidus vessels, those in the two chronic models revealed disrupted and attenuated elastica and intimal hyperplasia that was focal ("cushions") or generalized, leading to luminal occlusion. Variable numbers of cells in the tunica media of chronic nidus vessels contained smooth muscle actin. PC10/proliferating cell nuclear antigen immunoreactivity was observed in the endothelium and subendothelial layers. Histometry showed increases in intimal hyperplasia and medial thickness in the chronic vessels.**

CONCLUSION: **Nidus vessels in this chronic swine AVM model exhibited striking histologic changes similar to those seen in cerebral AVMs. The induced vessel growth seen angiographically and histologically in components of the chronic AVMs was consistent with the presence of persistently raised intravascular hemodynamic loads. This preliminary feasibility study suggests that the realistic histologic characteristics of this chronic AVM model are an attractive feature, and if confirmed in future, more comprehensive, studies would be of benefit in accurate histopathologic interpretation of the effects of superimposed experimental embolotherapy or radiosurgery. This model may provide a useful experimental tool to study the dynamic cellular and tissue events that dictate the development and natural history of AVMs.**

An acute-phase model of cerebral arteriovenous malformations (AVMs) was developed previously in swine, with a nidus fashioned from bilateral carotid retia mirabilia after surgical carotid-jugular fistula formation (1). True to the act of experimental model construction is the mandatory requirement of validation of this model by testing its accuracy (2); this is achieved by matching the model's behavior with known scientific observations about cerebral AVMs. In this respect, the realistic acute-phase angiographic and hemodynamic features of this model have been demonstrated previously (1, 3, 4).

The primary aim of this preliminary study was twofold: to assess the initial feasibility of maintaining live laboratory swine for variable periods after surgical carotid-jugular fistula formation and to

Received June 15, 1999; accepted after revision February 7, 2000.

From the Departments of Radiological Sciences (T.F.M., F.V., R.J.) and Pathology and Laboratory Medicine, Brain Research Institute (H.V.V., K.H.C.), UCLA School of Medicine and Medical Center, Los Angeles, CA.

Supported by grant RO1 HL/NS52352 from the National Institutes of Health.

Address reprint requests to Tarik F. Massoud, MD, Section of Neuroradiology, University Department of Radiology, Box 219, Cambridge University School of Clinical Medicine, Addenbrooke's Hospital, Hills Road, Cambridge CB2 2QQ U.K.

FIG 1. Anatomic basis and features of the swine AVM model.

A, Schematic representation of the normal left carotid arterial anatomy of the swine head and neck. The carotid rete mirabile is situated at the termination of the ascending pharyngeal artery. In the swine, the internal carotid artery is very short and joins the rete to the circle of Willis. *CC* indicates common carotid artery; *EC,* external carotid artery; *IM,* internal maxillary artery; *MM,* middle meningeal artery supplying the ramus anastomoticus; *RA,* ramus anastomoticus; *AA,* arteria anastomotica; *AP,* ascending pharyngeal artery; *O,* occipital artery; *BA,* basilar artery; *CW,* circle of Willis; *PC,* posterior cerebral artery; *MC,* middle cerebral artery; *AC,* anterior cerebral artery; *C,* ciliary artery; *EE,* external ethmoidal artery.

B, Schematic representation of the AVM model after creation of a right carotid–jugular fistula. *Arrows* indicate direction of flow; that is, from the left common carotid artery to both retia mirabilia (nidus) via the three feeding arteries (left ascending pharyngeal artery, left ramus anastomoticus, and left arteria anastomotica), and retrograde down the right ascending pharyngeal artery toward the right carotid-jugular fistula. Note balloon occlusion of the right external carotid artery.

C, Detail from a plastic cast of both carotid retia mirabilia of the swine shows the complex branching pattern of this microvascular bed. The surrounding nonvascular structures have been removed. *Arrows* indicate left and right ascending pharyngeal arteries. (Courtesy of Marc P. Ghysels, MD, Department of Medical Imaging, University of Liege, Belgium).

scrutinize further this swine model by examining the angiographic and histopathologic (light and electron microscopic, immunohistochemical, and histometric) changes in the nidus of chronic AVM models. It was intended that these preliminary investigations serve as an appropriate test of feasibility before engaging in future larger and more elaborate histopathologic studies that could help establish the basis for accurate histologic interpretation when using this chronic AVM model for laboratory testing and for the development of new embolization materials (5–7) or radiosurgical strategies (8) for cerebral AVMs. A secondary goal of the study was to gain some preliminary general insight into the histopathologic behavior of this model as a means of establishing the feasibility of 1) future, more extensive, studies to elucidate the temporal histopathologic transformation/evolution of the nidus microvasculature within this experimental AVM when exposed to varying and prolonged hemodynamic stresses (our ultimate goal in this respect is to be able to shed some light on mechanisms of cell and tissue proliferation in cerebral AVMs in relation to their underlying hemodynamic milieu); and 2) future studies that will attempt to assess the possible role of angiogenesis in the development of AVMs (9).

Methods

AVM Model Construction and Angiography

All animal experimentation was conducted in accordance with policies and guidelines set by the University Chancellor's Animal Research Committee and the National Institutes of Health. Seven Red Duroc swine were used in this study, three of which were used for histopathologic studies (see below). The animals were both male and female, were 3 to 4 months old, weighed 30 to 40 kg, and were maintained on a standard laboratory diet. After an overnight fast, each swine was premedicated with intramuscular 20 mg/kg of ketamine and 2 mg/kg of xylazine. General anesthesia was maintained with mechanical ventilation and inhalation of 1% to 2% halothane after endotracheal intubation.

The relevant vascular anatomy of the swine head and neck and the details of constructing the AVM model have been described previously (1) (Fig 1). After performing baseline angiography, a right side-to-side carotid-jugular fistula was constructed surgically using an aseptic technique, as described in prior reports. Additional occlusion of three side branches in the swine neck (right occipital artery, right external carotid artery, and muscular branch of the right ascending pharyngeal artery) was undertaken deliberately to ensure that shunting from the left to the right side of the neck was maximal across the AVM nidus in this long-term follow-up study, in which recruitment of many collateral pathways to the fistula would be expected over time. This optional maneuver is usually omitted in acute-phase uses of this model (3, 10). Immediate postoperative angiography was performed by selective injection of the left common carotid and ascending pharyngeal arteries to

demonstrate components of the AVM model and blood diversion through both retia (the nidus) toward the contralateral neck fistula. Subcutaneous tissues and skin were sutured in layers. During the procedure, the swine received prophylactic 0.9 to 1.2 $\times$ 10^6 units of penicillin G intramuscularly. Follow-up angiography on chronically maintained animals was performed similarly under general anesthesia to view the AVM model before the animals were killed.

Histopathology of the AVM Nidus

Vascular components of the AVM model were removed at autopsy in three animals. Euthanasia of the swine was performed using standard methods (pentobarbital 100 mg/kg intraarterially). At autopsy, a large incision was made in the calvaria and the brain was removed. Careful dissection of the parasellar dural reflections and within both cavernous sinuses revealed the underlying retia and the midline interretial connections. The AVM was removed in toto, and specimens were fixed by immersion in neutral buffered formalin or glutaraldehyde solutions. Specimens for light microscopy were embedded in paraffin or plastic and serial 5-μm-thick sections were obtained of paraffin-embedded specimens. Every fourth section was stained with hematoxylin-eosin before examination. Intervening sections were stained with elastica van Gieson, mucicarmine, which shows acidic epithelial mucosubstances (11), and periodic acid-Schiff stains for complex carbohydrates. Specimens for transmission electron microscopy were postfixed, washed, and dehydrated. They were then embedded in plastic and sectioned in thicknesses of 70 nm. These sections were mounted on grids and stained with lead citrate and uranyl acetate before examination using a Siemens electron microscope.

Immunohistochemical studies using monoclonal antibody to smooth muscle actin and PC10 antibody directed against a 36-kD cell cycle–regulated nuclear protein proliferating cell nuclear antigen (PCNA) were also performed in a standard fashion. For smooth muscle actin studies, paraffin sections (5-μm thick) on poly-L-lysine (0.01%) coated slides were deparaffinized, treated with 3% hydrogen peroxide in methanol to inhibit endogenous peroxidase activity, and hydrated. The slides were rinsed in 0.01 mol/L phosphate-buffered saline and blocked with 3% normal goat serum. Incubation with the monoclonal antibody to smooth muscle actin (Sigma Chemical Co, St Louis, MO) at 1:400 dilution was carried out overnight at 4°C. Control slides of adjacent sections were incubated with normal mouse serum in place of primary antiserum. A standard avidin-biotin peroxidase method was followed using biotinylated horse antimouse immunoglobulins (applied at 0.05 mg/mL) and an avidin-biotin complex. The peroxidase enzyme was visualized with the chromogen diaminobenzidine (0.01 mg/mL + 0.005% H_2O_2). The slides were lightly counterstained with hematoxylin-eosin, dehydrated, and mounted with coverslips. For PC10/PCNA studies, the procedure was as above except that the primary antiserum was PC10 (Novacastra, Newcastle-upon-Tyne, England) at 1:50 dilution. After three 5-minute rinses with phosphate-buffered saline, sections were incubated for 30 minutes with a secondary antibody (biotinylated horse antimouse) at 1:200 dilution, followed by a tertiary avidin-biotin complexed antibody. All sections were examined using a $\times$100 oil immersion lens mounted on an Olympus BH-2 microscope. However, quantification of proliferating cell populations (counting of smooth muscle and PC10/PCNA immunoreactive cells per unit area) was not carried out owing to the small sample size in this preliminary feasibility study.

Histometric Analysis of the AVM Nidus

Histologic sections stained with elastica van Gieson were selected and photographed for morphometry. Magnified copies of the photomicrographs (final magnification varied from $\times$160 to $\times$336) were projected and traced. For each of the three types of nidus vessels under investigation (acute, 2-month-old, and 6-month-old), a total of 18 vessels (selected at random from right and left retia) were traced, and measurements of these (corrected for magnification) were performed with the aid of an automated image analyzer (Zeiss Interactive Digital Analysis System, Carl Zeiss, Inc., Thornwood, NY) to reveal the circumference of the vessel lumen (in mm), the length of the internal elastic lamina (in mm), and the circumference of the outer margin of the media (in mm). From these, the following parameters were calculated automatically and their means ($\pm$ SD) derived: the area of the vessel lumen (in mm^2), the entire area enclosed by the internal elastic lamina (in mm^2), the area of intimal hyperplasia (in mm^2), the entire area enclosed by the outer margin of media (in mm^2), the area of the media (in mm^2), the medial thickness (in mm), and the radius of the vessel (in mm). The results of histometric analysis were examined qualitatively for general trends. Statistical analysis was not possible owing to the small number of specimens in this preliminary study.

Results

All swine tolerated the general anesthesia and the surgical and endovascular procedures with no ill effects. One model was created for use in the acute phase. The other six swine were kept for follow-up, during which all the animals appeared normal, with no obvious ill effects.

Immediate postoperative angiography showed a successful acute-phase simulation of an AVM in all swine. Upon selective injection of the left common carotid artery or ascending pharyngeal artery, a very rapid angiographic sequence was observed in each model: orthograde flow in the left ascending pharyngeal artery (main feeder), shunting through both retia mirabilia across the midline (nidus), and rapid retrograde flow down the right ascending pharyngeal artery and common carotid artery (main draining vein) to the fistula (Fig 2A). Beyond the fistula, opacified blood in the external jugular vein dispersed mostly in an orthograde direction.

Follow-up angiography in six swine was performed from days 2 to 180 after surgery: one swine at day 2, one swine at day 4, two swine at day 14, one swine at day 56 (shown in Fig 2B), and one swine at day 180 (shown in Fig 2C). The persistent increased blood flow through each AVM model resulted in progressive dilatation (see sizes below) and tortuosity (judged subjectively) of its main arterial feeder and draining vein. This vascular dilatation was evident as early as day 4 after AVM creation, and was maximal in the 6-month-old model (Fig 2C). The main feeder and draining veins were considerably dilated in the most chronic models, attaining sizes similar to that of the normal external carotid artery in the swine (normally, the ascending pharyngeal artery [about 2 mm in diameter] is less than half the size of the external carotid artery [5 mm]). In addition, unlike the normally straight ascending pharyngeal artery, these AVM components became elongated and tortuous, a reflection of the long-term increased intravascular hemodynamic load. On the other hand, angiographic changes in the microvessels of the AVM nidus

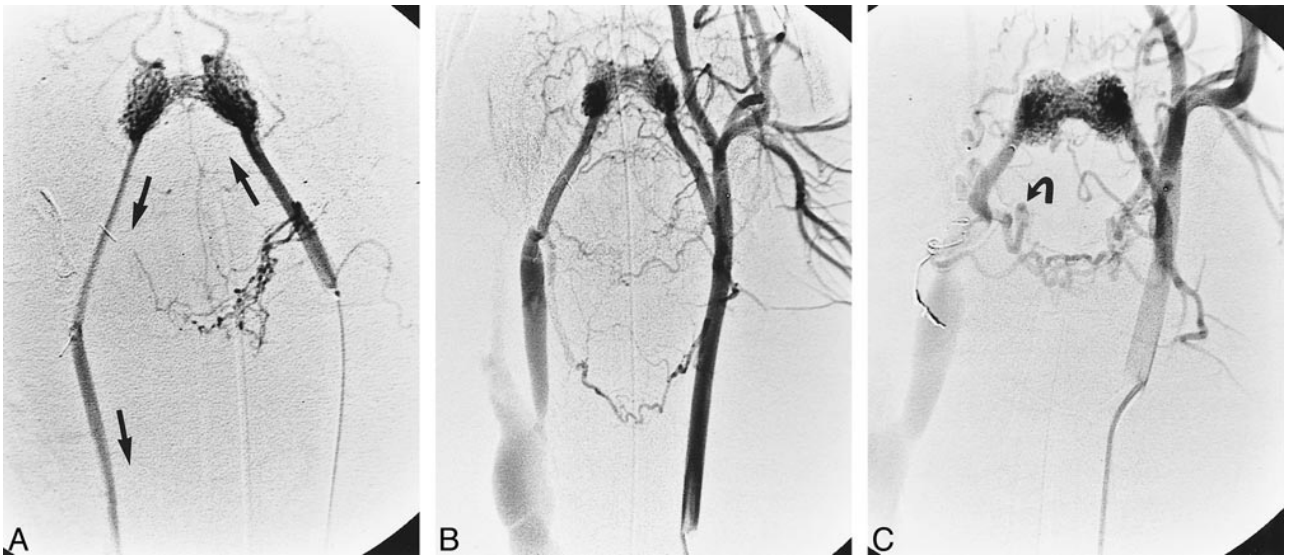

FIG 2. *A,* Frontal view of a superselective left ascending pharyngeal arteriogram shows rapid shunting flow through the AVM nidus and retrograde flow in the draining vein portion of the AVM down toward the carotid-jugular fistula immediately after model construction. Straight coils were used to occlude right-sided neck branches during model construction. *Arrows* indicate direction of flow.

B, Frontal left common carotid arteriogram shows features of the same AVM model as in *A* but 2 months later. Note dilatation and some elongation of the component vessels as well as marked dilatation of the external jugular vein.

C, Frontal left common carotid arteriogram shows features of the 6-month-old AVM model. Note dilatation and elongation of its component vessels and the overall coarse pattern of nidus microvessels. In this swine, the muscular branch of the right ascending pharyngeal artery (*arrow*) was not occluded during model construction owing to temporary vasospasm, which prevented access. This allowed the delayed recruitment of blood via anastomoses with the namesake contralateral artery, in parallel with shunting across the AVM nidus.

were more difficult to assess by measurements of vascular caliber, because the size of individual microvessels was just beyond the size limit for digital subtraction angiographic resolution. Nevertheless, these were judged subjectively to show a probable increase in caliber and an overall coarser vascular pattern, especially in the most chronic models.

Among the six swine followed up beyond the acute period, histopathologic studies were conducted on one 2-month-old and one 6-month-old AVM nidus. In addition, nidus histology of the acutely created AVM model acted as a control specimen (Fig 3). The decision to analyze histopathologically only three of the seven swine in this study was made a priori. Owing to the preliminary feasibility nature of this study, it was thought that examination of one swine at each end of the experimental follow-up period and one swine as close to halfway through this period as possible would be sufficient to gain the intended glimpse of possible trends in histopathologic observations. Although analysis of all seven swine would have been marginally more useful, it was thought that this small number would still be insufficient to provide statistically relevant data. Clearly, the small number of experimental subjects used in this study precludes the formation of solid conclusions. However, on the basis of these preliminary results, our future goal is to launch a more comprehensive study with a larger number of experimental animals examined at greater intervals with the aim of achieving statistically significant results.

Light microscopic findings in the acute model were as described previously in the literature (also see below) for the normal swine rete mirabile (12–14). Light microscopy of the chronic nidi revealed striking changes, many of which were similar to those encountered in human AVM specimens. These included disrupted and attenuated elastica with overlying focal intimal hyperplasia (ie, intimal cushions or endoluminal pads of Conti [15]), severe intimal thickening (which in places produced complete luminal occlusion), and mucicarmine-positive ground substance among cells of hyperplastic intima. The 6-month-old nidus vessels were generally of larger caliber and more ectatic, with noticeable segments of mural thinning, and the intimal cushions appeared somewhat less prominent than in the 2-month-old nidus; however, intimal hyperplasia was measurably increased on histometry (see below). None of the above changes was observed in the acute model (ie, the normal retial microvesels).

Electron micrographs of the chronic model vessels were markedly abnormal (Fig 4), displaying thinning and attenuation of the endothelium with focal breaks or gaps in the endothelial barrier. Underlying fibromuscular hyperplasia was noted with prominent smooth muscle and fibroblast cells, which were separated by bands of collagen and granular and fibrillar material, probably representing glycosaminoglycans. The internal elastic lamina was disrupted.

Immunohistochemical studies showed that variable numbers of cells in the tunica media contained

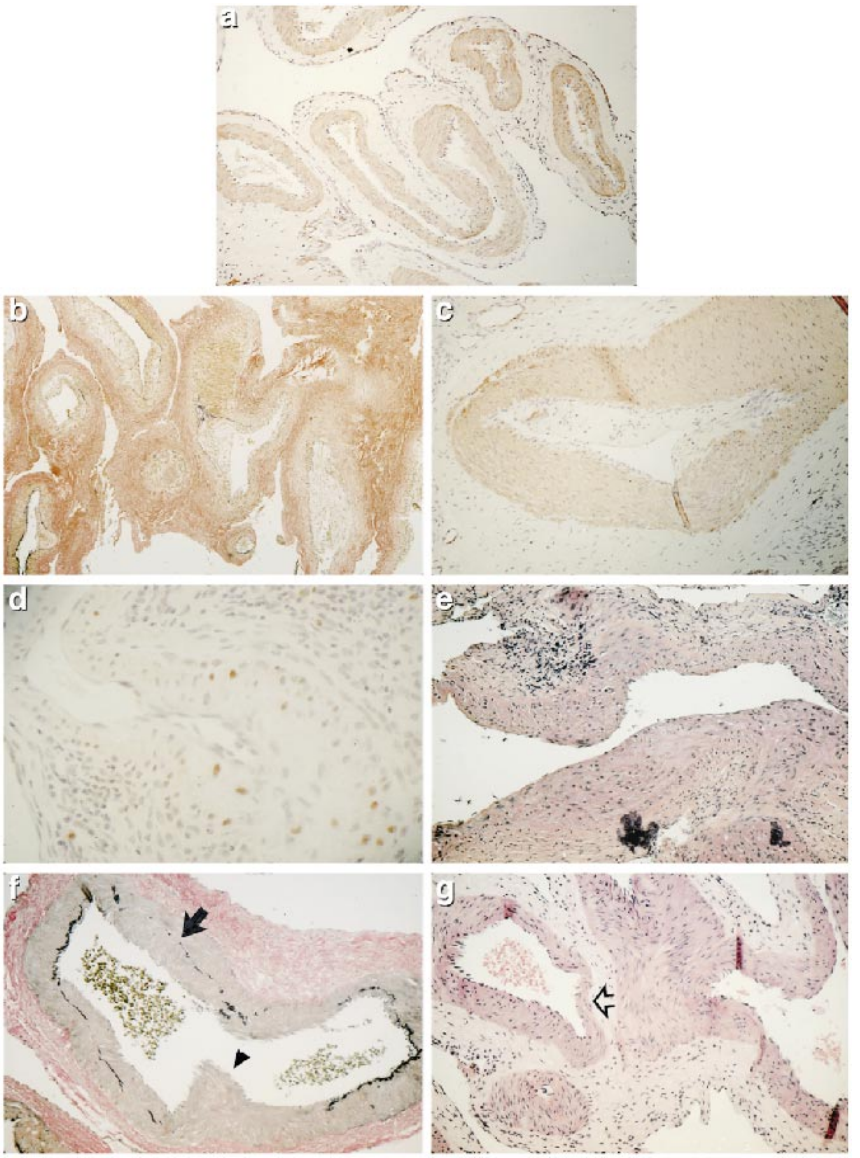

FIG 3. Histologic and immunohistochemical features of the swine AVM models.

A, Immunohistochemical features of the nidus microvessels in the acute AVM model (ie, of normal rete mirabile microvessels) using monoclonal antibody to smooth muscle actin, followed by counterstaining with hematoxylin-eosin. Original magnification ×40.

B, Histologic section of the 2-month-old nidus vessels after staining with elastica van Gieson. Note the prominent intimal hyperplasia that occludes vessels in places and prominent disruption of the elastica. Original magnification ×16.

C, Immunohistochemical features of the nidus microvessels in the 2-month-old AVM model using monoclonal antibody to smooth muscle actin, followed by counterstaining with hematoxylin-eosin. Note medial thickening and intimal hyperplasia. Original magnification ×40.

D, Immunohistochemical features of the nidus microvessels in the 2-month-old AVM model using PC10 antibody to PCNA followed by counterstaining with hematoxylin-eosin. Note widespread presence of proliferating cells. Original magnification ×104.

E, Histologic section of the 2-month-old nidus vessels after staining with mucicarmine. Note the mucicarmine-positive ground substance among cells of hyperplastic intima. Original magnification ×40.

F, Histologic section of the 6-month-old nidus vessels after staining with elastica van Gieson. Note the multifocal destruction of the elastica layer (*arrow*) and the intimal hyperplasia in the form of an endoluminal cushion (*arrowhead*). Original magnification ×40.

G, Histologic section of the 6-month-old nidus vessels after staining with hematoxylin-eosin. Note the focal segments of mural thinning (*arrow*). Original magnification ×40.

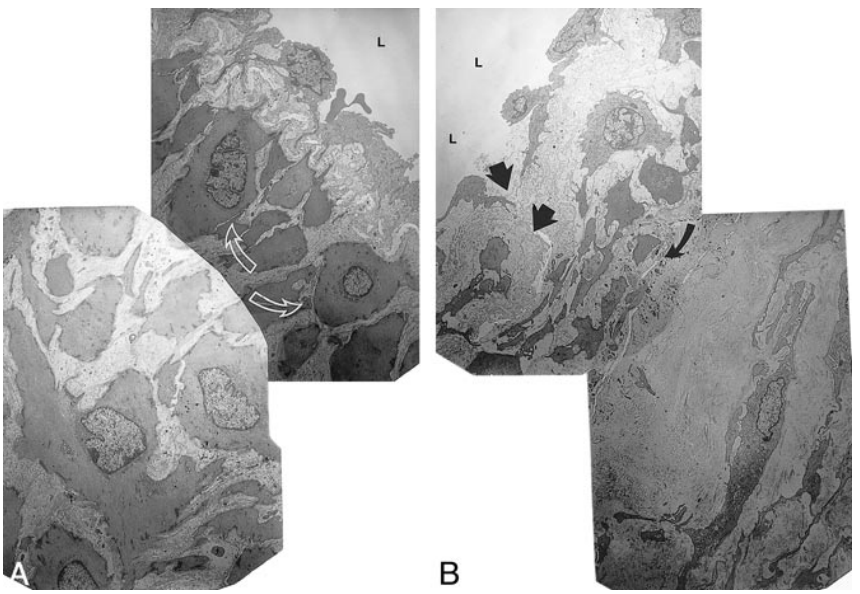

FIG 4. Electron micrographs of nidus vessels in the acute AVM model (ie, of normal rete mirabile microvessels) (*A*) and in the 2-month-old AVM model (*B*). *L* indicates vessel lumen. Original magnifications ×7500.

A, Note the normal and variably prominent endothelium. Smooth muscle cells (*arrows*) are immediately deep to the internal elastic lamina.

B, Note thinning and attenuation of the endothelium with focal breaks in the endothelial barrier (*straight arrows*). Underlying fibromuscular hyperplasia is noted with prominent smooth muscle and fibroblast cells, which are separated by bands of collagen and granular and fibrillar material, probably representing glycosaminoglycans. *Curved arrow* indicates a focus in which the internal elastic lamina is attenuated.

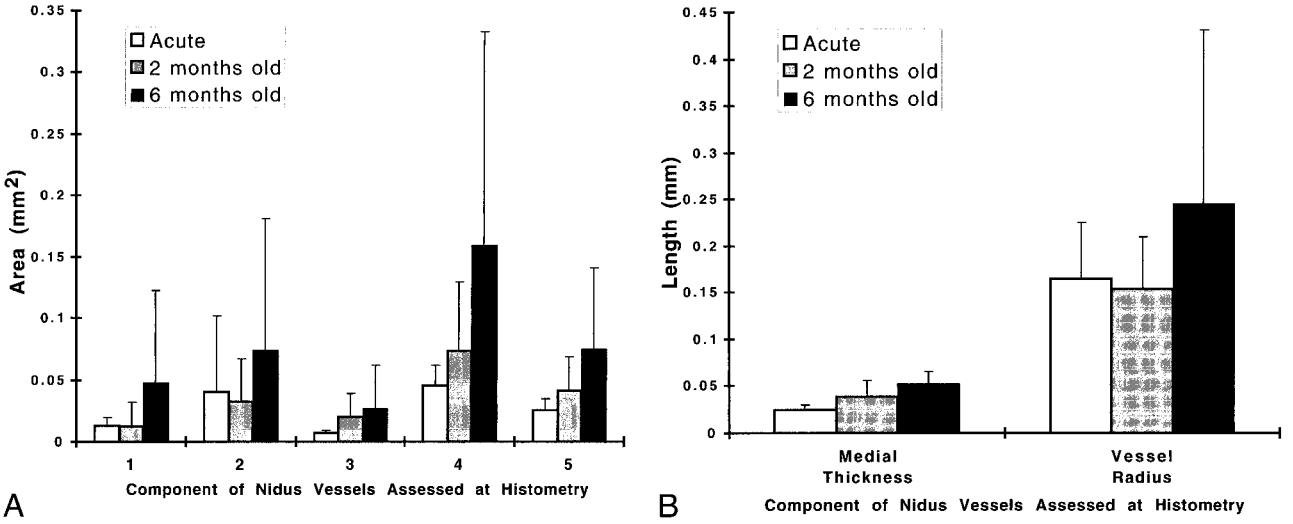

FIG 5. *A,* Histogram of mean values (± SD) for five histometric parameters that characterize various areas (in mm²) of the nidus microvessels when measured in the acute, 2-month-old, and 6-month-old AVM models. The five parameters were 1) area of the vessel lumen, 2) entire area enclosed by the internal elastic lamina, 3) area of intimal hyperplasia, 4) entire area enclosed by the outer margin of media, and 5) area of media.

B, Histogram of mean values (± SD) for the medial thickness and vessel radius (in mm) of the nidus microvessels when measured in the acute, 2-month-old, and 6-month-old AVM models.

smooth muscle actin; these were more prominent in the vessels of the chronic nidus. PC10/PCNA immunoreactivity was observed in the endothelium and subendothelial layers, but no obvious qualitative difference in immunoreactivity was found between the acute and chronic nidus microvessels (Fig 3).

The results of histometric measurements are shown in Figure 5. The diameter of the nidus vessel averaged 328 μm in the acute model and 490 μm (ie, twice the obtained vessel radius) in the swine kept for 6 months. The 6-month-old vessels displayed the largest measurements and calculations of medial thickness, vessel radius, and areas. Particularly prominent were the increases in intimal hyperplasia and medial thickness seen in the chronic models.

Discussion

Several striking transmural microscopic changes in chronic AVM nidus vessels were observed in this preliminary study. These included attenuated or destroyed elastica, marked intimal hyperplasia, vessel dilatation, areas of mural thinning, and ultrastructural abnormalities in the endothelium and subendothelium. Despite the preliminary nature of this study, its findings are useful on two fronts. First, they reveal that the chronic swine AVM model is likely to be useful when performing histopathologic studies of new embolic agents or experimental radiosurgery, because the histologic effects of these interventions would be superimposed on a background of realistic histologic changes representative of cerebral AVMs. However, a more concrete and reliable confirmation of this likelihood could only be obtained in future studies using many more experimental subjects. The present study establishes the feasibility of this line of investigation. Second, these initial findings lend indirect support to hypotheses suggesting that many of the complex histopathologic features observed in human AVMs are secondary to hemodynamic stresses induced by high intravascular blood flow (16).

Histology and Immunohistochemistry of Cerebral AVMs

The combination of primary and acquired histologic features (see below) in the nidus of cerebral AVMs is usually revealed as numerous enlarged and abnormal artery-like and vein-like channels (17) with intervening unidentifiable types of vessels (15, 18–23). Artery-like microvessels usually contain a well-defined internal elastic lamina, although the elastica may be split or focally deficient in some areas. Vein-like microvessels usually contain no discernible elastica, but may be markedly thickened. The endothelium is thickened and projects into the lumen as endoluminal pads of Conti (15). Some vascular channels within an AVM show localized smooth muscle hyperplasia, possibly at sites of platelet-fibrin thrombus deposition that may be determined by hemodynamic factors. Thrombosis may occlude the vessels, or the thrombi may be mural with ensuing organization. Calcification is often present in AVM vessel walls, but frank complicated atherosclerosis with ulceration is rarely seen in AVM channels. The extravascular neural parenchymal component of an AVM also shows characteristic features: abundant evidence of old hemorrhage is often present, and extensive gliosis is frequently encountered within brain tissue. Ul-

trastructural study of AVMs reveals myofibrillary aggregates with densities within smooth muscle cells; endothelial gaps are present; and subendothelial basement membranes are thick, reticulated, or multilaminated (17, 24, 25).

The assessment of cellular proliferation in histologic material is a valuable component of conventional histopathologic analysis. Methods that permit in situ assessment of cellular proliferation, such as immunohistochemistry, are preferable to methods that require disruption of tissues, such as flow cytometry (26). A particular advantage is that the immunohistologic demonstration of cell cycle–related antigens allows spatial orientation to be shown, and the phenotype of proliferating cells can be determined by double staining methods. Smooth muscle cells in vessels of cerebral AVMs have been studied previously using a monoclonal antibody against the muscle protein actin (22). Similar studies on smooth muscle cell proliferation have been performed in vein of Galen malformations (27) and in AVMs previously treated by embolization (28). Cell proliferation can also be assessed in formalin-fixed, paraffin-embedded tissue using monoclonal antibody PC10 directed against PCNA (28). PCNA is the cofactor of DNA polymerase delta, an enzyme required for DNA replication (29). The rate of synthesis of PCNA correlates directly with the proliferative state of cells. Using this method, investigators have analyzed patterns of endothelial proliferation over embolization material in AVM vessels (28). Quantitative immunohistochemical analysis (ie, cell counts per unit area) was not performed in this preliminary study owing to the small number of specimens examined. Future, more extensive, studies using these immunohistochemical techniques could provide us with a more dynamic picture of cellular events in this experimental AVM model and in cerebral AVMs.

Swine AVM Model

Past experimental in vivo studies of AVMs have been hampered by the lack of an appropriate animal model that possesses a representative AVM nidus. Therefore, a limited perspective of histopathologic reactions in vessels subjected to arteriovenous shunting has been available only from such models as experimental large arteriovenous fistulas in sheep (30) and rabbits (16). In these, changes in the dilated and tortuous arterial limbs resulted in frequent interruptions of the internal elastic lamina, medial thinning, and intimal proliferation. Changes in the venous portion of the fistulas consisted of marked intimal thickening, loose intimal proliferation of smooth muscle, deposition of metachromic extracellular material, and loss or extensive fragmentation of elastica. In chronic models, venous intimal tears resulted in the accumulation of mural thrombi and eventual mural fibrosis.

These histopathologic observations in large experimental arteriovenous fistulas provide some indication of vessel reaction when subjected to hemodynamic stress. However, a more accurate experimental replication of events within a human AVM nidus would be expected if experimental shunting were possible through microvessels of the same caliber as those of a human nidus. The carotid rete mirabile of the swine consists of a compact plexus of intertwining microarteries with an angiographic appearance similar to a plexiform human AVM nidus (14). The average diameter of normal rete vessels was reported previously by Lee et al (13) to be 154 μm, although it is unclear if this represented only the luminal diameter. In this study, the diameter (including mural thickness) was 328 μm. The reason for this disparity is unclear, but, conveniently, both are comparable to the size of human AVM nidus vessels, which in one study were shown to have an average diameter of 265 μm (20). Histologically, however, the normal rete microarteries are relatively thick-walled relative to human AVMs. Light microscopy reveals a well-defined undulating internal elastic lamina and a predominantly muscular tunica media with an average thickness of 36 μm, as reported previously by Brothers et al (12), or of 25 μm, as seen in this study.

Bilateral retia mirabilia of the swine were successfully incorporated into an in vivo experimental AVM model. The normal swine carotid rete mirabile possesses relatively low blood flow owing to a small drop in intravascular pressure between its afferent and efferent arteries. On the other hand, cerebral AVMs possess high shunting flow induced by significant arteriovenous pressure gradients. Thus, the AVM model was created by diverting (from one side of the neck to the other, across the midline) and increasing blood flow through bilateral retia after surgical formation of a large unilateral carotid-jugular fistula (1, 3, 4).

One important limitation of this AVM model accurately is its position at the skull base within both cavernous sinuses; therefore, unlike cerebral AVMs, it is not close to or surrounded by brain tissue. Histopathologic effects on adjacent brain parenchyma cannot be reproduced using this model. Nevertheless, the model offers several advantages: 1) it is simple to construct (10); 2) it possesses an accessible, intact, and fast-flowing nidus; 3) it possesses feeders and draining veins that are easy to catheterize and to observe at angiography; 4) the degree of blood shunting across the nidus is variable, thus simulating a spectrum of low- and high-flow AVMs; 5) en bloc removal of the AVM model is possible at animal autopsy, thus allowing histologic examination of its vascular components; and 6) as demonstrated for the first time in this study, the model can be maintained for a chronic period, thereby enabling the performance of temporal angiographic and vascular histopathologic studies.

A significant benefit of this AVM model is its replication of the hemodynamic features of simple cerebral AVMs. In previous studies using this mod-

el, it was observed that an average arteriovenous pressure gradient of 28 mm Hg exists across the nidus (4), and the average peak flow velocity falls across the nidus from 63.4 ± 24.6 cm/s in the main feeder to 38.9 ± 13.7 cm/s in the main draining vein (3). Hemodynamic assessments of swine were not conducted in the present preliminary study, but it would appear reasonable to assume that similar hemodynamic conditions were present in the AVM models under investigation. The ability to establish the prevailing hemodynamic conditions across the nidus of this AVM model accurately represents a significant advantage that will be made use of in future larger studies to correlate the model's histologic findings with its hemodynamic features.

Histomorphogenesis of AVM Microvessels

Cerebral AVMs are highly dynamic rather than static entities (31). They are constantly subjected to circulatory mechanical forces and to a variety of pathologic alterations that progressively transform them into complex vascular anomalies. Most AVMs do not become symptomatic until the third decade of life. It is logical, therefore, to conclude that these lesions undergo morphologic and hemodynamic changes even after the brain has reached maturity. Marin–Padilla (31) has stated that ''... it should be of great significance in the study of these malformations to be able to distinguish and to separate their primary or original features from the secondary or acquired ones.''

The abnormal morphogenetic evolution of AVMs (ie, the dynamic cellular and tissue events that dictate their development and natural history) has been speculated upon but remains unknown. The lack of this knowledge stems in part from the inability to perform such dynamic investigations on human AVM specimens, from the near absence of naturally occurring animal models of AVMs, and from the previous lack of in vivo experimental models of AVMs. The availability of the described swine AVM model now provides a potential tool for investigating this issue. The interesting results of this preliminary study will form a springboard for future more extensive studies to elucidate the temporal histopathologic transformation/evolution of the nidus microvasculature within this experimental AVM model and to correlate these changes with detailed hemodynamic parameters prevailing across the nidus.

Some precursory observations relevant to this issue of AVM histomorphogenesis can be made from the findings of this study. For example, the dilatation and elongation of the arterial feeder and nidus vessels observed at angiography and histometry in the more chronic AVM models are consistent with the observations of Nornes and Grip (32) in cerebral AVM feeders. They postulated that this vessel growth could arise after two possible hemodynamic triggers: low intraluminal pressure and high flow velocity. Both triggers have been shown previously to be integral features of this swine AVM model (3, 4). It is known that lowering of blood pressure tends to reduce tangential wall tension and results in vessel dilatation (33). It has been suggested that endothelial cell membrane potential changes associated with higher flow (either via shear stress–activated channels or stretch-activated channels) may regulate blood vessel tone via direct action on underlying smooth muscle cells (34). Dilatation may then result from electrical coupling (hyperpolarization transmitted to the smooth muscle cells) or by release of potent vasorelaxants, such as endothelial-derived relaxing factor (34).

The observed thickening of nidus vessels (medial and intimal) in chronic models is most likely due to the persistent effects of increased disturbed flow and regions of low shear stress (near bifurcations and curved segments) present in this highly intertwining vascular structure (35). Oscillations in the direction of wall shear stress are also likely to contribute to the marked formation of intimal hyperplasia (36, 37). The noted increase in medial thickness seen in the more chronic nidus vessels suggests at first the presence of an underlying hypertensive angiopathy (38, 39). This finding is difficult to interpret precisely, given the known lower mean pressure values (compared with values in the normal state before surgery) in the arterial feeder and draining vein, and the presence of a pressure gradient across the AVM nidus. One possibility is that this may be more a reflection of the frequent occurrence of zones of low shear stress causing vascular thickening in a highly complex bifurcating network of microvessels.

The swine model used did not replicate the ''metamorphotic proliferative angiodysplasia or capillaropathy'' that would appear to characterize the primary disease process in the embryologic genesis of AVMs (25); this occurs at approximately the third week of gestation in humans (40). Therefore, the histologic appearance of these changes alone remain unknown. Nevertheless, the prominent and realistic histologic transformations seen in the swine microvessels due to high blood flow suggest that these induced or secondary features might play a preeminent role in shaping the final histopathologic picture of cerebral AVMs as observed in surgical or autopsy specimens.

It is tempting to postulate various molecular mechanisms or pathways by which our observed histopathologic transformations might occur as a result of hemodynamic stress. Such an analysis, however, is beyond the scope of this preliminary investigation. What is known is that mechanical forces associated with blood flow play an important role in the regulation of vascular structure and remodeling (41). Significant regulation of blood vessel responses occurs by the action of hemodynamic shear stress on the endothelium. In turn, flow-mediated endothelial mechanotransduction leads to biophysical, biochemical, and gene regulatory responses (41). Characterization of growth factor ex-

pression within nidus microvessels of this AVM model will be undertaken in future, more comprehensive, studies. By an extension of this line of experimentation we believe that this approach may help toward an understanding of the possible role of angiogenesis in high-flow vascular beds (9) and, eventually, the potential development of antiangiogenic adjunctive therapy for cerebral AVMs (42).

Acknowledgments

We are grateful to the staff of the Leo G. Rigler Research Laboratory at UCLA for their technical support, and to Mari-Anne Akers for performing the electron microscopy.

References

1. Massoud TF, Ji C, Viñuela F, et al. **An experimental arteriovenous malformation model in swine: anatomic basis and construction technique.** *AJNR Am J Neuroradiol* 1994;15:1537–1545
2. Massoud TF, Hademenos GJ, Young WL, Gao E, Pile-Spellman J, Viñuela F. **Principles and philosophy of modeling in biomedical research.** *FASEB J* 1998;12:275–285
3. Murayama Y, Massoud TF, Viñuela F. **Transvenous hemodynamic assessment of experimental arteriovenous malformations: Doppler guidewire monitoring of embolotherapy in a swine model.** *Stroke* 1996;27:1365
4. Murayama Y, Massoud TF, Viñuela F. **Hemodynamic changes in arterial feeders and draining veins during embolotherapy of arteriovenous malformations: an experimental study in a swine model.** *Neurosurgery* 1998;43:96–106
5. Massoud TF, Ji C, Viñuela F, et al. **Laboratory simulations and training in endovascular embolotherapy using a swine arteriovenous malformation model.** *AJNR Am J Neuroradiol* 1996;17:271–279
6. Massoud TF, Ji C, Guglielmi G, Viñuela F. **Endovascular treatment of arteriovenous malformations with selective intranidal occlusion by detachable platinum electrodes: technical feasibility in a swine model.** *AJNR Am J Neuroradiol* 1996;17:1459–1466
7. Massoud TF, Hademenos GJ. **Transvenous retrograde nidus sclerotherapy under controlled hypotension (TRENSH): a newly proposed treatment for brain arteriovenous malformations: concepts and rationale.** *Neurosurgery* 1999;45:351–365
8. De Salles AAF, Solberg T, Mischel P, et al. **Arteriovenous malformation animal model for radiosurgery: the rete mirabile.** *AJNR Am J Neuroradiol* 1996;17:1451–1458
9. Rothbart D, Awad IA, Lee J, Kim J, Harbaugh R, Criscuolo GR. **Expression of angiogenic factors and structural proteins in central nervous system vascular malformations.** *Neurosurgery* 1996;38:915–925
10. Massoud TF. **Experimental arteriovenous malformation modeling in laboratory sheep versus swine [letter].** *AJNR Am J Neuroradiol* 2000;21:985–988
11. Laurén PA, Sorvari TE. **The histochemical specificity of mucicarmine staining in the identification of epithelial mucosubstances.** *Acta Histochem* 1969;34:263–272
12. Brothers MF, Kaufmann JCE, Fox AJ, Deveikis JP. **N-butyl-cyanoacrylate: substitute for IBCA in interventional neuroradiology.** *AJNR Am J Neuroradiol* 1989;10:777–786
13. Lee DH, Wriedt CH, Kaufmann JCE, Pelz DM, Fox AJ, Viñuela F. **Evaluation of three embolic agents in pig rete.** *AJNR Am J Neuroradiol* 1989;10:773
14. Lylyk P, Viñuela F, Vinters HV, et al. **Use of a new mixture for embolization of intracranial vascular malformations: preliminary experimental experience.** *Neuroradiology* 1990;32:304–310
15. Paillas JE, Berard M, Sedan R. **The relative importance of atheroma in the clinical coarse of arteriovenous angioma of the brain.** In: Luyendijk, W, ed. *Cerebral Circulation (Special Issue of Prog Brain Res)*1968;30:419
16. Pile-Spellman JMD, Baker KF, Liszczak TM, et al. **High-flow angiopathy: cerebral blood vessel changes in experimental chronic arteriovenous fistula.** *AJNR Am J Neuroradiol* 1986;7:811–815
17. Martin N, Vinters H. **Pathology and grading of intracranial vascular malformations.** In: Barrow DL, ed. *Intracranial Vascular Malformations: Neurosurgical Topics.* Park Ridge, Ill: American Association of Neurological Surgeons;1990;1–31
18. Dandy WE. **Arteriovenous aneurysm of the brain.** *Arch Surg* 1928;17:190–243
19. Hamby WB. **The pathology of supratentorial angiomas.** *J Neurosurg* 1957;22:65–75
20. Isoda K, Fukuda H, Takamura N, Hamamoto Y. **Arteriovenous malformation of the brain: histological study and micrometric measurement of abnormal vessels.** *Acta Pathol Jpn* 1981;31:883–893
21. Leu HJ. **Pathomorphology of vascular malformations.** *Int Angiol* 1990;9:147–154
22. Mandybur TI, Nazek M. **Cerebral arteriovenous malformations: a detailed morphological and immunohistochemical study using actin.** *Arch Pathol Lab Med* 1990;114:970–973
23. Russell DS, Rubenstein LJ. ***Pathology of Tumors of the Nervous System.*** Baltimore: Williams & Wilkins;1971;9–102
24. Meyermann R, Yasargil MG. **Ultrastructural findings in the intima of vessels of cerebral angiomas gained operatively.** In: Cervos-Navarro J, Fritschka E, eds. *Cerebral Microcirculation and Metabolism.* New York; Raven;1981;473
25. Yasargil MG. **Pathological considerations.** In: Yasargil MG, ed. *Microneurosurgery.* Stuttgart: Thieme;1987;49–56
26. Hall PA, Levison DA. **Assessment of cell proliferation in histological material.** *J Clin Pathol* 1990;43:184–192
27. Reichman A, Viñuela F, Duckwiler GR, Peacock WJ, Vinters HV. **Pathologic findings in a patient with a vein of Galen aneurysm treated by staged endovascular embolization.** *Childs Nerv Syst* 1993;9:33–38
28. Schweitzer JS, Chang BS, Madsen P, et al. **The pathology of arteriovenous malformations of the brain treated by embolotherapy, II: results of embolization with multiple agents.** *Neuroradiology* 1993;35:468–474
29. Cobb MA, Husain M, Andersen BJ, Al-Mefty O. **Significance of proliferating cell nuclear antigen in predicting recurrence of intracranial meningioma.** *J Neurosurg* 1996;84:85–90
30. Stehbens WE. **Blood vessel changes in chronic experimental arteriovenous fistulas.** *Surg Gyn Obstet* 1968;127:327–331
31. Marin-Padilla M. **Embryology.** In: Yasargil MG, ed. *Microneurosurgery.* Stuttgart: Thieme;1987;23–47
32. Nornes H, Grip A. **Hemodynamic aspects of cerebral arteriovenous malformations.** *J Neurosurg* 1980;53–456
33. Zarins CK, Zatina MA, Giddens DP, Ku DN, Glagov S. **Shear stress regulation of artery lumen diameter in experimental atherogenesis.** *J Vasc Surg* 1987;5:413–420
34. Davies PF, Dull RO. **How does the arterial endothelium sense flow? Hemodynamic forces and signal transduction.** In: Diana JN, ed. *Tobacco Smoking and Atherosclerosis.* New York; Plenum Press;1990;281–293
35. Matsuda I, Niimi H, Moritake K, Okumura A, Handa H. **The role of hemodynamic factors in arterial wall thickening in the rat.** *Atherosclerosis* 1978;29:363–371
36. Ku DN, Giddens DP, Zarins CK, Glagov S. **Pulsatile flow and atherosclerosis in the human carotid bifurcation.** *Arteriosclerosis* 1985;5:293–302
37. Morinaga K, Okadome K, Kuroki M, Miyazaki T, Muto Y, Inokuchi K. **Effect of wall shear stress on intimal thickening of arterially transplanted autogenous veins in dogs.** *J Vasc Surg* 1985;2:430–433
38. Owens GK, Reidy MA. **Hyperplastic growth response of vascular smooth muscle cells following induction of acute hypertension in rats by aortic coarctation.** *Circ Res* 1985;57:695–705
39. Schwartz SM, Reidy MA. **Common mechanisms of proliferation of smooth muscle in atherosclerosis and hypertension.** *Hum Pathol* 1987;18:240–247
40. Mayer PL, Kier EL. **The ontogenetic and phylogenetic basis of cerebrovascular anomalies and variants.** In: Apuzzo MLJ, ed. *Brain Surgery: Complication Avoidance and Management.* New York: Churchill Livingstone;1993;691–792
41. Davies PF. **Flow-mediated endothelial mechanotransduction.** *Physiol Rev* 1995;75:519–560
42. Megyesi JF, Findlay JM. **Expression of angiogenic factors and structural proteins in central nervous system vascular malformations [comment].** *Neurosurgery* 1996;38:925